

# Gain-of-Function *Lrp5* Mutation Improves Bone Mass and Strength and Delays Hyperglycemia in a Mouse Model of Insulin-Deficient Diabetes

Giulia Leanza,<sup>1,5</sup>  Francesca Fontana,<sup>1</sup> Seung-Yon Lee,<sup>1</sup> Maria S. Remedi,<sup>3</sup> Céline Schott,<sup>2,4</sup> Mathieu Ferron,<sup>2,4</sup>  Malcolm Hamilton-Hall,<sup>1</sup> Yael Alippe,<sup>1</sup> Rocky Strollo,<sup>5</sup> Nicola Napoli,<sup>1,5</sup>  and Roberto Civitelli<sup>1</sup> 

<sup>1</sup>Division of Bone and Mineral Diseases, Department of Medicine, Musculoskeletal Research Center, Washington University School of Medicine, St. Louis, MO, USA

<sup>2</sup>Molecular Physiology Research Unit, Institut de Recherches Cliniques de Montréal, Montréal, Quebec, Canada

<sup>3</sup>Division of Endocrinology, Metabolism and Lipid Research, Department of Medicine, Washington University School of Medicine, St. Louis, MO, USA

<sup>4</sup>Molecular Biology Programs & Department of Medicine, Université de Montréal, Montréal, Quebec, Canada

<sup>5</sup>Department of Medicine, Unit of Endocrinology and Diabetes, Campus Bio-Medico University of Rome, Rome, Italy

## ABSTRACT

High fracture rate and high circulating levels of the Wnt inhibitor, sclerostin, have been reported in diabetic patients. We studied the effects of Wnt signaling activation on bone health in a mouse model of insulin-deficient diabetes. We introduced the sclerostin-resistant *Lrp5*<sup>A214V</sup> mutation, associated with high bone mass, in mice carrying the *Ins2*<sup>Akita</sup> mutation (Akita), which results in loss of beta cells, insulin deficiency, and diabetes in males. Akita mice accrue less trabecular bone mass with age relative to wild type (WT). Double heterozygous *Lrp5*<sup>A214V</sup>/Akita mutants have high trabecular bone mass and cortical thickness relative to WT animals, as do *Lrp5*<sup>A214V</sup> single mutants. Likewise, the *Lrp5*<sup>A214V</sup> mutation prevents deterioration of biomechanical properties occurring in Akita mice. Notably, *Lrp5*<sup>A214V</sup>/Akita mice develop fasting hyperglycemia and glucose intolerance with a delay relative to Akita mice (7 to 8 vs. 5 to 6 weeks, respectively), despite lack of insulin production in both groups by 6 weeks of age. Although insulin sensitivity is partially preserved in double heterozygous *Lrp5*<sup>A214V</sup>/Akita relative to Akita mutants up to 30 weeks of age, insulin-dependent phosphorylated protein kinase B (pAKT) activation in vitro is not altered by the *Lrp5*<sup>A214V</sup> mutation. Although white adipose tissue depots are equally reduced in both compound and Akita mice, the *Lrp5*<sup>A214V</sup> mutation prevents brown adipose tissue whitening that occurs in Akita mice. Thus, hyperactivation of Lrp5-dependent signaling fully protects bone mass and strength in prolonged hyperglycemia and improves peripheral glucose metabolism in an insulin independent manner. Wnt signaling activation represents an ideal therapeutic approach for diabetic patients at high risk of fracture. © 2021 The Authors. *Journal of Bone and Mineral Research* published by Wiley Periodicals LLC on behalf of American Society for Bone and Mineral Research (ASBMR).

**KEY WORDS:** Lrp5; WNT SIGNALING; BONE; DIABETES; BROWN ADIPOSE TISSUE

## Introduction

The incidence of type 1 diabetes (T1D) and type 2 diabetes (T2D) is increasing worldwide, whereas improvements in diabetes treatment have contributed to an exponential increase in the number of fragility fractures in these patients. Indeed, low-trauma fractures now substantially contribute to deterioration of quality of life and mortality in diabetic patients, in addition

to vascular complications.<sup>(1,2)</sup> However, the mechanisms by which diabetes exposes patients to high risk of low-trauma fractures remain only partly known. The modestly lower bone mineral density (BMD) cannot entirely explain the several-fold higher fracture rate in T1D patients relative to age-matched controls,<sup>(3)</sup> and BMD is even higher than normal in T2D, after adjustment for body size.<sup>(4,5)</sup> Low bone turnover is common among T2D and T1D, although histologic studies in T1D are

This is an open access article under the terms of the Creative Commons Attribution-NonCommercial-NoDerivs License, which permits use and distribution in any medium, provided the original work is properly cited, the use is non-commercial and no modifications or adaptations are made.

Received in original form August 13, 2020; revised form March 21, 2021; accepted March 28, 2021; Accepted manuscript online April 8, 2021.

Address correspondence to: Nicola Napoli, MD, PhD, Unit of Endocrinology and Diabetes, Università Campus Bio-Medico, Via Alvaro del Portillo, 21, 00128 Roma, Italy. Email: n.napoli@unicampus.it

Additional Supporting Information may be found in the online version of this article.

*Journal of Bone and Mineral Research*, Vol. 36, No. 7, July 2021, pp 1403–1415.

DOI: 10.1002/jbmr.4303

© 2021 The Authors. *Journal of Bone and Mineral Research* published by Wiley Periodicals LLC on behalf of American Society for Bone and Mineral Research (ASBMR).

not all consistent with decreased bone formation.<sup>(6,7)</sup> Subtle defects in bone microarchitecture and increased accumulation of advanced glycosylation end-products (AGEs) and pentosidine, which alter bone stiffness, have been reported in T1D subjects.<sup>(8)</sup> Abnormal accumulation of AGEs in bone has also been observed in a rat model of T1D.<sup>(9)</sup> High glucose concentration in extracellular fluids and AGEs can increase expression of the Wnt inhibitor, sclerostin, and decrease receptor activator of NF- $\kappa$ B ligand (RANKL) production in vitro, potentially explaining the low bone turnover in T1D.<sup>(10)</sup> Consistent with these observations, we have recently shown that circulating glycated hemoglobin is positively associated with increased fracture rate in T1D patients.<sup>(11)</sup>

Canonical Wnt signaling is a key modulator of bone homeostasis. In humans, gain-of-function mutations of the *LRP5* Wnt co-receptor gene are associated with high bone mass.<sup>(12,13)</sup> Likewise, loss-of-function mutations of *SOST*, the gene encoding sclerostin, cause sclerosteosis or van Buchem disease, both high bone mass disorders.<sup>(14,15)</sup> Importantly, an anti-sclerostin antibody, romosozumab, has been recently approved for use in the United States and other countries for increasing bone mass and reducing fracture risk in osteoporosis.<sup>(16)</sup> Mounting evidence suggests that the Wnt signaling pathway, and sclerostin in particular, might be implicated in the mechanisms leading to low bone formation and suboptimal bone quality of diabetes patients. Increased circulating sclerostin has been observed in subjects with T1D<sup>(17)</sup> and T2D, where it is inversely correlated with bone turnover markers, but is positively associated with BMD.<sup>(18–22)</sup> Indeed, we have recently found that *SOST* expression is increased in bone of T2D patients.<sup>(23)</sup> Preclinical studies further suggest that Wnt signaling is involved in glucose metabolism. Mice with a null mutation of the *Lrp5* gene are osteopenic and glucose intolerant.<sup>(24,25)</sup> By contrast, *Sost* knockout mice have higher insulin sensitivity and lower adiposity than normal littermates,<sup>(26)</sup> in addition to high bone mass.<sup>(27)</sup>

Based on this background, we used mouse genetic models to ask whether activating Wnt signaling may counteract the bone and metabolic abnormalities that develop in insulin-dependent diabetes. Results confirm that a sclerostin-insensitive *Lrp5* mutant leads to high bone mass accrual and improved bone strength in mice with prolonged, severe hyperglycemia. Importantly, the gain-of-function *Lrp5* mutation delays the onset of hyperglycemia and prevents whitening of brown adipose tissue that occurs in insulin-deficient mice. Our studies suggest that therapies based on Wnt activation may be beneficial to both bone and glucose homeostasis.

## Materials and Methods

### Animals

Mice carrying the germline *Lrp5*<sup>A214V</sup> mutant allele, which results in high bone mass (HBM) phenotype,<sup>(28)</sup> were a generous gift from Dr. Matthew L. Warman (Harvard University, Boston, MA, USA). The *Lrp5*<sup>A214V</sup> mutation renders the receptor insensitive to antagonists, particularly sclerostin, which consequently hyperactivates Wnt signaling.<sup>(29)</sup> *Ins2*<sup>Akita</sup> (Akita) mice were purchased from Jackson Laboratories (Stock number 003548; Bar Harbor, ME, USA). These mice carry one mutant *Ins2* allele that causes insulin protein misfolding, cellular stress, and eventual apoptosis of beta cells, thereby leading to spontaneous hyperglycemia by 4 to 5 weeks of age in males.<sup>(30)</sup> Heterozygous *Lrp5*<sup>+/A214V</sup> (HBM) mice were mated with *Ins2*<sup>Akita</sup> mice, to obtain, in one generation, double heterozygous *Lrp5*<sup>+/A214V</sup>;*Ins2*<sup>Akita</sup> (HBM/Akita) mice, as well as single

heterozygous and wild-type (WT) mice. All the mouse lines used in this project were bred in a C57BL/6J background, and littermates were used as controls. Mice were weaned at postnatal day 28 (P28), fed a regular chow and housed in a room maintained at constant temperature (25°C) on a 12-h light and 12-h dark cycle. Genotyping for *Lrp5* was performed via polymerase chain reaction (PCR) on genomic DNA extracted from mouse tails using the HotSHOT method,<sup>(31)</sup> and primers to detect the WT and *Lrp5*<sup>A214V</sup> alleles, as described.<sup>(28)</sup> Genotyping for the *Ins2*<sup>Akita</sup> allele was performed by TransnetYX, Inc. (Cordova, TN, USA). Tissues for postmortem analysis (adipose tissue depots, pancreas) were collected immediately after euthanasia. Brown adipose tissue (BAT) was extracted from the intrascapular region; white adipose tissue was harvested from gonadal/inguinal and retroperitoneal areas (gWAT, rWAT, respectively). Tissues were snap frozen in liquid nitrogen until processing. All animal procedures were performed in accordance with procedures approved by the Institutional Animal Care and Use Committee of Washington University in St. Louis (Protocols number 20140279, 20170095, and amendments).

### Body composition analysis

To determine whole-body composition, dual-energy x-ray absorptiometry (DXA) was performed using a Faxitron UltraFocus100 scanner (Faxitron Bioptics, LLC, Tucson, AZ, USA) at different ages. Mice were anesthetized by 2% isoflurane inhalation, a concentration that has no impact on metabolic parameters,<sup>(32)</sup> and placed in a prone position on an imaging-positioning tray. Whole-body scans were made excluding head and tail. Analyses included whole-body BMD, bone mineral content (BMC), percent body fat, and lean mass. The instrument was calibrated daily before use, and one investigator (Giulia Leanza) performed all scans.

### BAT histology

The entire BAT depot was excised from the intrascapular region of 30-week-old mice, fixed in ethanol, and processed for paraffin inclusion. Sections were stained with hematoxylin and eosin and imaged by bright-field microscopy (NanoZoomer; Hamamatsu Photonics K.K., Hamamatsu, Japan). Sections from four blocks, each from a different mouse, were analyzed per genotype.

### Bone microarchitecture

For in vivo longitudinal analysis of bone microarchitecture, mice were scanned at 6 and 20 weeks of age at the proximal tibia by micro-computed tomography ( $\mu$ CT) (VIVA CT40; SCANCO Medical AG, Brüttsellen, Switzerland) as described.<sup>(33)</sup> Before scanning, the leg was fully extended, while the mouse was kept in a mask to ensure the continuous flow of 2% isoflurane during the entire procedure. The leg was immobilized in the scanner using a custom designed fixture, so as to minimize any variability due to leg repositioning. Microstructural analysis of trabecular and cortical bone was also performed as described.<sup>(33)</sup> For ex vivo  $\mu$ CT analysis, tibias or femurs were stored at  $-20^{\circ}\text{C}$  until use, then placed in 2% agarose gel and scanned using a  $\mu$ CT-40 system (SCANCO Medical AG) as described.<sup>(34)</sup>

### Bone biomechanics

For assessment of bone strength, dissected tibias were tested in three-point bending to failure or fracture using methods described.<sup>(33)</sup> Briefly, specimens were stabilized over two

supports placed 7 mm apart in an Instron 8841 apparatus (Instron, Norwood, MA, USA). A loading force was applied in the anteroposterior direction midway between the two supports by a displacement ramp at a rate of 0.03 mm/s. Force and displacement data were collected at 100 Hz (Labview 5.0; National Instruments, Austin, TX, USA), and test curves were analyzed as described.<sup>(35)</sup>

### Glucose metabolism

Capillary blood was obtained by cutting 1 to 2 mm of tissue from the tail tip with sharp scissors, and glucose measurements were performed using the On-call Express Blood Glucose Meter (ACON Laboratories, San Diego, CA, USA). Because the detection limit of this device is 600 mg/dl, blood glucose above this level was recorded as 600 mg/dl but considered to be a lower limit of the true value.<sup>(36)</sup> Intraperitoneal glucose tolerance test (ipGTT) was performed after 6 h morning or 14 h overnight fasting on conscious mice. Glucose sampling was obtained at baseline and 15, 30, 45, 60, 90, and 120 min after an intraperitoneal glucose injection (1.5 g/kg dextrose in 50% solution).<sup>(37)</sup> Insulin tolerance test (ITT) was performed at 7 weeks of age after 6 h morning fasting. Insulin (0.5 U/kg body weight) was administered intraperitoneally<sup>(38)</sup>; blood glucose was obtained at baseline and 15, 30, 45, 60, 90, and 120 min after insulin injection.

### Circulating hormones

Blood samples were drawn from the tail vein in heparinized capillary tubes during an ipGTT at time 0, immediately before dextrose injection, and 30 min after injection. Serum insulin, glucagon, and C-peptide were measured using Millipore Sigma's MILLIPLEX MAP Mouse Metabolic Hormone Magnetic Bead Panel - Metabolism Multiplex Assay MMHMAG-44K (Millipore Sigma, Burlington, MA, USA), containing beads for insulin, glucagon, and C-peptide 2 (Washington University Immunoassay Core, St. Louis, MO, USA). Insulin-like growth factor 1 (IGF-1) was measured using mouse IGF-1 (BR55) LXSAMSM 1plex (R&D Systems, Minneapolis, MN, USA) by the Washington University Immunoassay Core. Glu, Gla13, and total mouse osteocalcin were measured using three specific enzyme-linked immunosorbent assays (ELISAs), as described<sup>(39)</sup> by two co-authors (Mathieu Ferron, Céline Schott). Briefly, 96-well ELISA plates (R&D Systems) were coated with anti-Glu-osteocalcin, anti-Gla13-osteocalcin, or anti-Mid-osteocalcin antibodies diluted in coating buffer (Immunochemistry Technologies, Bloomington, MN, USA) and incubated overnight at room temperature. Then, the plates were washed and blocked with assay diluent (0.1% Tween and 3% bovine serum albumin [BSA] in phosphate buffered saline [PBS]) for 4 h at room temperature. Afterward, standards or serum samples was added to assay diluent and plates were sealed and incubated overnight at 4°C. The Gla13 and total osteocalcin (OCN) (Mid) ELISA were run using synthetic 3XGla-OCN (Bio-Synthesis Inc., Lewisville, TX, USA) as standard, whereas Glu-OCN ELISA was run using bacterial produced Glu-OCN as standard. After five washes, horseradish peroxidase-conjugated anti-CT-osteocalcin (osteocalcin C-terminus) antibody was added to each well and placed on a shaker for 1 h at room temperature. After further washes, the plates were incubated with the substrate, tetramethylbenzidine (Pierce, Rockford, IL, USA) for 15 min. The reaction was stopped with 100 µl of HCl 1M and detected by

colorimetry at 450 nm wavelength in a microplate reader. Polynomial second-order standard curves were used to determine the concentration of Glu (undercarboxylated), Gla13 (carboxylated), and total osteocalcin. Glu13 was calculated by subtracting Gla13 from total osteocalcin.

### Whole-pancreas insulin content

After euthanasia, the pancreas was isolated, weighted (wet weight), then minced and homogenized using a mechanical homogenizer in acid/ethanol extraction buffer (77% 100 proof ethanol, 1.5% HCl; 1 ml/100 mg tissue). The extract was incubated overnight at 4°C and centrifuged at 400g for 30 min at 4°C. Supernatants were stored at -20°C until analysis. Insulin content was determined by ELISAs at 1:5000 dilution, as detailed.<sup>(36)</sup>

### Adipocyte cultures

Adipocyte cultures were prepared from external ear stromal cells following an established procedure.<sup>(40)</sup> External ears were collected and cut in small pieces in ice-cold Hank's balanced salt solution (HBSS) containing antibiotics; incubated in 2 mg/ml collagenase I (Worthington Biochemical Corp., Lakewood, NJ, USA) for 1 h at 37°C, filtered through a 70-µm cell strainer (BD Biosciences, San Jose, CA, USA) and pelleted by centrifugation at 189 relative centrifugation force (RCF) (1300 revolutions per minute (rpm)) for 10 min. Cells were re-suspended, seeded, and subcultured in Dulbecco's modified Eagle medium (DMEM)/Ham's F-12 Nutrient Mixture (F12) containing 15% fetal bovine serum (FBS) and 10 ng/ml fibroblast growth factor (FGF). Confluent cultures were incubated in adipogenic medium (5 µg/ml insulin, 1 µM dexamethasone, 500 µM isobutyl-methylxanthine, 5 µM rosiglitazone; Sigma, St. Louis, MO, USA) for 2 days; switched to DMEM/F12 with 10% FBS, 5 µg/ml insulin and 5 µM rosiglitazone for 2 days; then cultured in DMEM/F12 with 10% FBS and visually monitored until accumulation of lipid droplets. For the signaling experiments, cells were incubated in serum-free media for 2 h before exposure to insulin.

### Immunoblots

Protein extracts were prepared by lysing cells cultured in six-well plates with radioimmunoprecipitation assay (RIPA) buffer (50mM Tris, 150mM NaCl, 1mM ethylenediamine tetraacetic acid [EDTA], 0.5% NaDOAc, 0.1% sodium dodecylsulfate [SDS], and 1.0% NP-40) plus a phosphatase and protease inhibitor cocktail (Xpert P3200-001 and P3100-001; GenDEPOT, Katy, TX, USA). Protein concentration was determined by the Bio-Rad method (DC Protein Assay), and equal amounts of proteins were subjected to SDS-polyacrylamide gel electrophoresis (SDS-PAGE) gels (8–15%). Proteins were transferred onto polyvinylidene fluoride (PVDF) membranes and incubated overnight with primary antibody at 4°C, followed by a 1-h incubation with secondary goat anti-mouse or goat anti-rabbit Alexa-Fluor 680 (Molecular Probes, Eugene, OR, USA), or donkey anti-goat 780 (LI-COR Biosciences, Lincoln, NE, USA) antibody. Primary antibodies include total protein kinase B (Akt), phospho-Akt (Ser473) (Cell Signaling Technology, Beverly, MA, USA) and β-actin (Santa Cruz Biotechnology, Santa Cruz, CA, USA). The results were visualized using Li-Cor Odyssey Infrared Imaging System (LI-COR Biosciences).

## Data presentation and statistical analysis

Group data are presented in box-plots with median and interquartile range; whiskers represent maximum and minimum values. When appropriate, arithmetic mean is shown as plus sign within the box-plot. Unless otherwise noted, repeated measures are plotted as median and interquartile range. Differences between groups were assessed using one-way analysis of variance (ANOVA), and repeated measures were analyzed by two-way ANOVA or mixed-effects models, in cases of missing data points, followed by Tukey's tests to adjust *p* values for multiple comparisons. Data were managed in Microsoft Excel (Microsoft Corp., Redmond, WA, USA), plotted, and analyzed using Prism 8.0 and 9.1 (GraphPad Software, San Diego, CA, USA).

## Results

The *Lrp5*<sup>A214V</sup> mutation results in high whole-body bone mass and prevents BAT whitening, but not loss of WAT in the Akita background

Validating the *Lrp5*<sup>A214V</sup> model, whole-body BMD and BMC measured by DXA were significantly higher in the HBM groups relative to either the Akita or control groups up to at least 26 weeks of age (Figure 1A,B), whereas body weight and length were not different among the four experimental groups (Figure 1, Supplemental Figure S1A,B). Aside a slightly lower BMD at 6 weeks in HBM/Akita mice, there were no differences in whole-body bone mass between double and single HBM

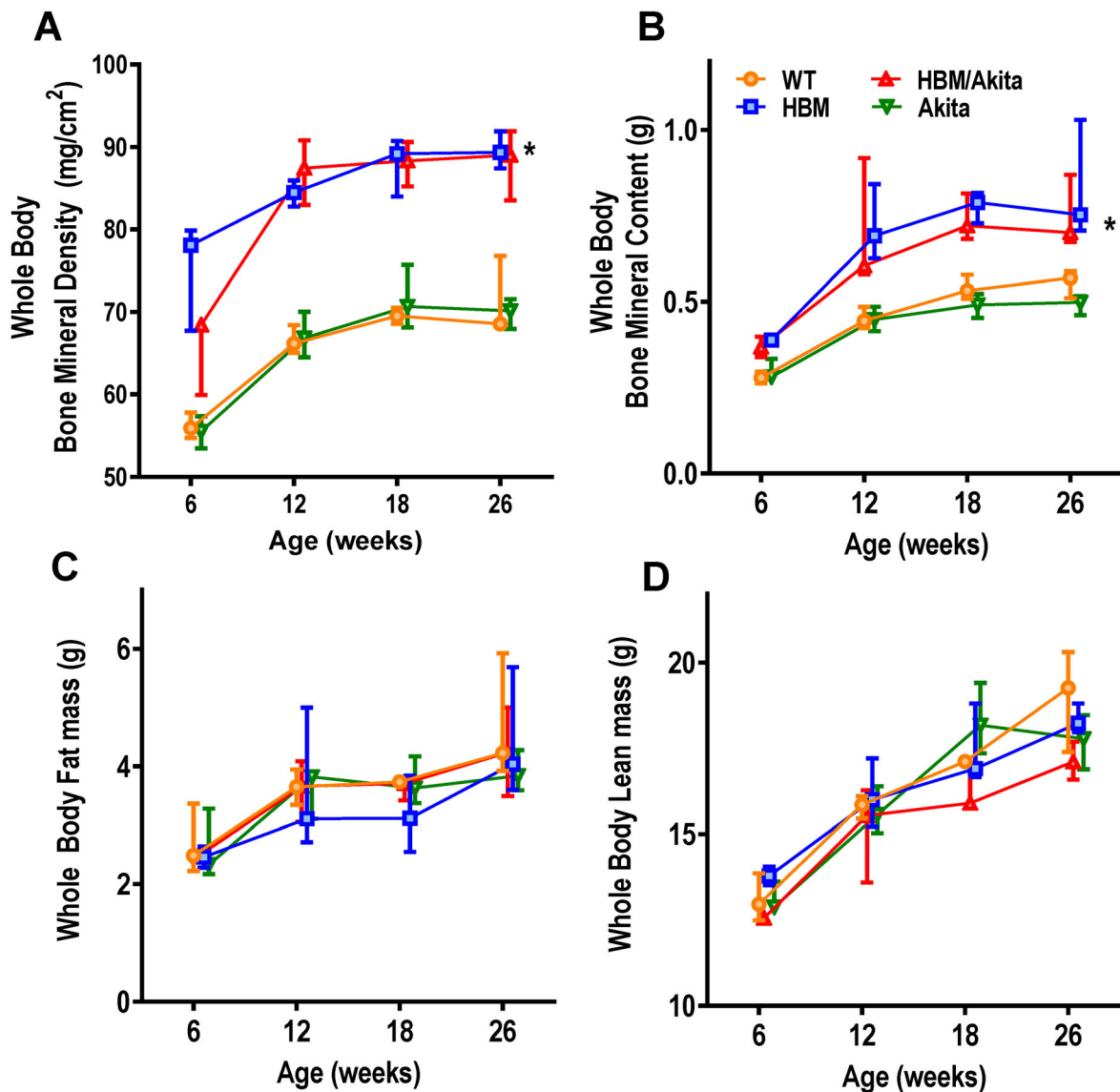


**Fig. 1.** Body composition analysis. (A) Whole-body bone mineral density, (B) bone mineral content, (C) fat mass, and (D) lean mass measured by DXA at different ages in the different mutants. *n* = 3–7 at 6 weeks, 6–11 at 12 weeks, *n* = 3–6 at 18 weeks, *n* = 5–7 at 26 weeks. Asterisk indicates *p* < .001 for HBM and HBM/Akita versus WT and Akita at all time points, except for HBM/Akita at 6 weeks, when *p* > .10 versus all other groups (adjusted *p* values by Tukey's multiple comparison test after two-way ANOVA). Abbreviations: ANOVA, analysis of variance; DXA, dual-energy x-ray absorptiometry; HBM, high bone mass; WT, wild-type.

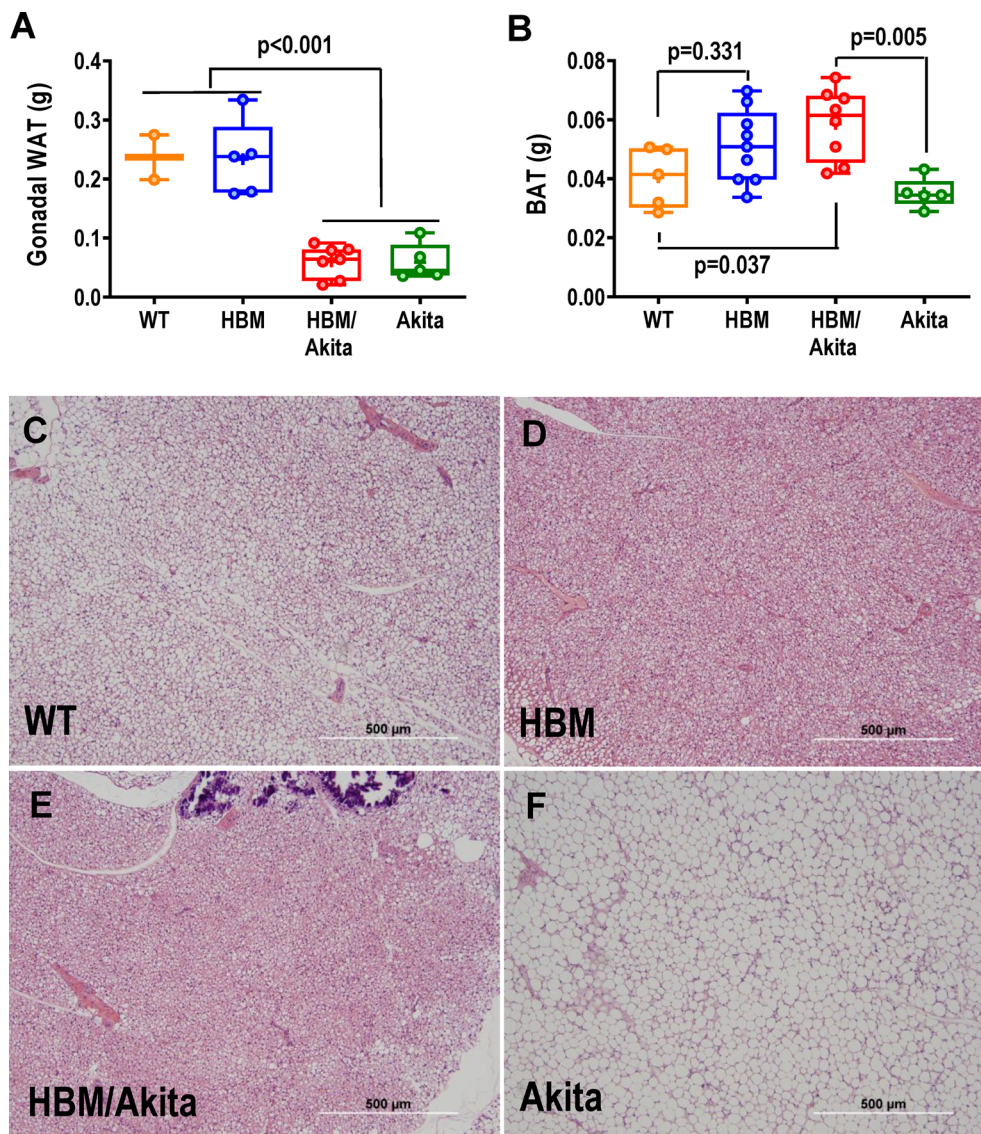


**Fig. 2.** Fat tissue mass and histology. (A) Gonadal WAT, and (B) suprascapular BAT mass determined postmortem at 30 weeks of age. Brackets indicate adjusted  $p$  values (Tukey's multiple comparison test) after one-way ANOVA; in A, brackets indicate comparison of all groups on one side with all groups on the other side. (C–F) H&E-stained sections of BAT representative of the four genotype groups at 30 weeks of age. Abbreviations: ANOVA, analysis of variance; BAT, brown adipose tissue; H&E, hematoxylin and eosin; WAT, white adipose tissue.

mutants. Likewise, analysis of whole-body fat and lean mass by DXA showed no significant differences among groups at the different time points (Figure 1C,D). However, direct postmortem assessment of fat depots revealed significantly lower gonadal and retroperitoneal WAT accumulation in both Akita and double mutants relative to the other two groups (Figure 2A, Figure 1, Supplemental Figure S1C). By contrast, BAT mass was significantly higher in HBM/Akita mice relative to both WT and Akita groups; median BAT mass was also higher in HBM than in WT, but the groups did not significantly differ (Figure 2B). Histological sections of BAT revealed denser cellularity and reduced number of lipid droplet-containing cells in HBM and HBM/Akita (Figure 2D,E), relative to WT BAT (Figure 2C). By contrast, BAT isolated from Akita mice was almost entirely constituted by lipid containing adipocytes (Figure 2F). Thus, the HBM mutation increases BAT mass and prevents BAT whitening in Akita mice.

### The *Lrp5*<sup>A214V</sup> mutation improves bone microarchitecture and preserves bone strength in the Akita background

In vivo analysis of bone microarchitecture by  $\mu$ CT confirmed higher volumetric trabecular bone volume/total volume (BV/TV) and BMD in both HBM and HBM/Akita mutants relative to WT and Akita at 6 and 20 weeks of age (Figure 3A–C). Of note, the difference between WT and HBM groups was significant only at 20 weeks, reflecting increasing BV/TV and BMD with age in HBM and HBM/Akita mice, relative to minimal changes in WT and Akita mice (Figure 3B,C). Accordingly, trabecular thickness was higher and trabecular spacing lower in both HBM groups relative to WT and Akita (Figure 3, Supplemental Figure S2A,B). Also, trabecular thickness increased with age in both HBM groups, without changes in trabecular spacing, consistent with bone mass accrual with age in these groups. Again, only minor age-

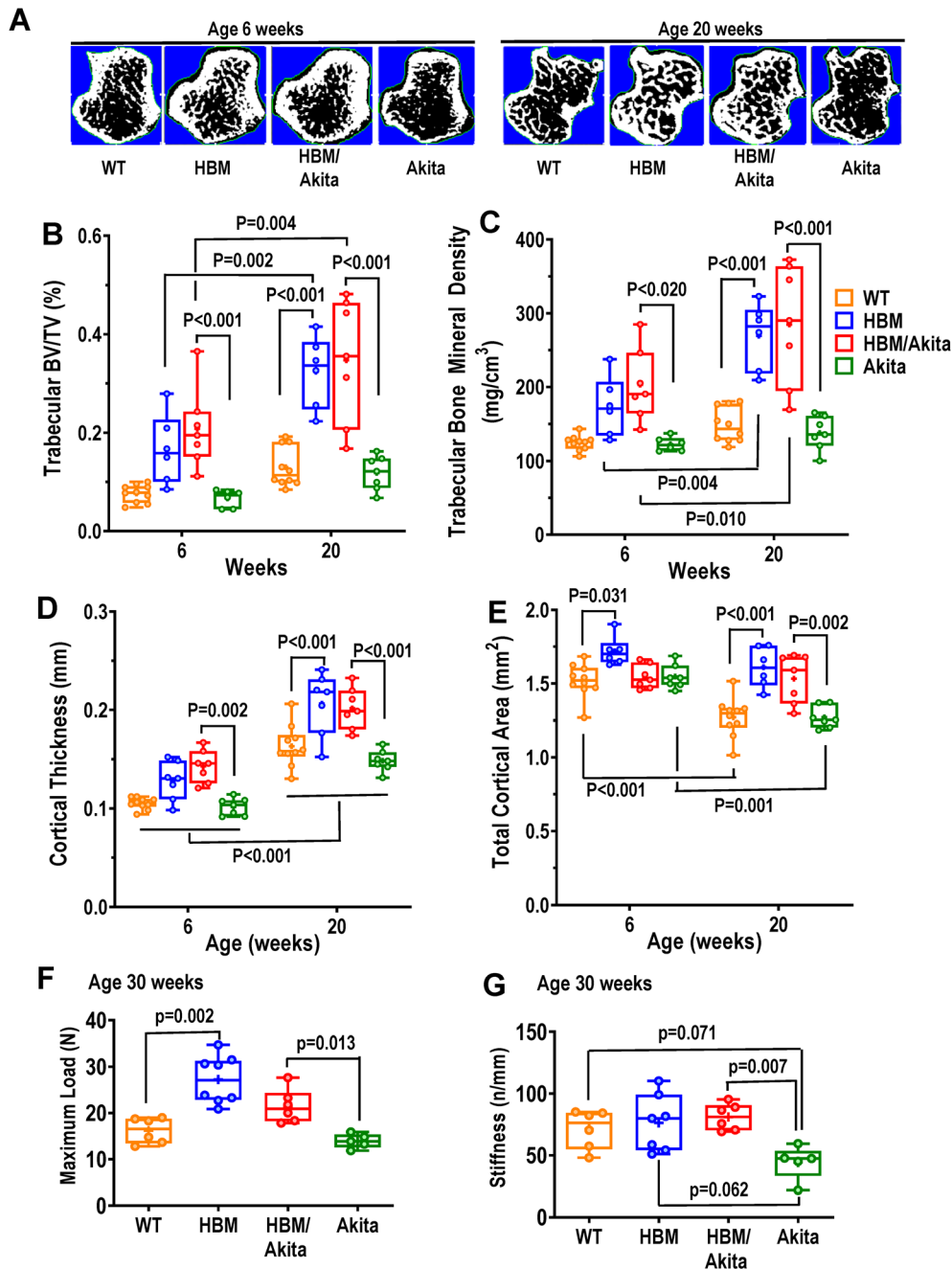


**Fig. 3.** Bone microarchitecture and biomechanics. (A) Cross-sections of proximal tibias from in vivo  $\mu$ CT scans representative of the four experimental groups at 6 and 20 weeks of age. (B) Volumetric trabecular BV/TV, (C) trabecular bone mineral density, (D) cortical thickness, and (E) total cortical area in the four genotype groups at two different ages. (F) Maximum load, and (G) stiffness derived from three-point bending analysis of femurs at 30 weeks of age. Brackets indicate adjusted  $p$  values (Tukey's multiple comparison test) after two-way ANOVA (B–E), or one-way ANOVA (F,G). Brackets on multiple groups (D) indicate pairwise comparison of each genotype group at 6 and 20 weeks. Pairwise comparisons with  $p > .10$  are not indicated. Abbreviations:  $\mu$ CT, micro-computed tomography; ANOVA, analysis of variance; BV/TV, bone volume/total volume.

related trends were observed in trabecular thickness and spacing in the WT and Akita groups (Figure 3, Supplemental Figure 2A,B). As for trabecular bone, cortical thickness and cortical bone area were also higher in both HBM mutants relative to both WT and Akita groups at both ages and increased in all group with age (Figure 3D, Figure 3, Supplemental Figure S2C). Total cortical area, representing bone cross-sectional size, was

higher in HBM than in WT at 6 weeks, but it was not different between HBM/Akita and Akita mutants; however, both HBM groups did not experience the decline in total cortical area that occurred in WT and Akita, resulting in larger cross-sectional area in the HBM mutants at 20 weeks (Figure 3E). Consistent with increased cortical thickness, medullary area decreased with age in all groups, without evident genotype effect (Figure 3,

Supplemental Figure S2D). Tissue mineral density, which represents the degree of mineralization, was higher in trabecular bone of both HBM groups at 6 weeks, but this difference disappeared at 20 weeks; and both trabecular and cortical tissue mineral density increased with age in all groups rather uniformly (Figure 3, Supplemental Figure S2E,F).

We then assessed bone biomechanical properties in femurs from a subset of mice followed until age 30 weeks. As anticipated, maximum load in a three-point bending was significantly higher in HBM relative to WT bones, and in HBM/Akita relative to Akita mice, whereas no difference was observed between Akita and WT mice (Figure 3F). On the other hand, bone stiffness was significantly lower in Akita compared to all other groups, although the difference was below the significance threshold only relative to HBM/Akita double mutants, most likely because of low power (Figure 3G). Microarchitectural parameters determined *ex vivo* in these 30-week-old mice subjected to bone strength testing confirmed high volumetric BV/TV and BMD, cortical thickness and bone area in HBM and HBM/Akita relative to the other groups, but no significant differences were noted between Akita and WT (Figure 3, Supplemental Figure S3A–D).

The *Lrp5*<sup>A214V</sup> mutation delays the onset of hyperglycemia and glucose intolerance in Akita mice

We monitored glucose homeostasis to validate the Akita model and correlate with the skeletal phenotype. Although blood glucose in WT and HBM mice was normal and stable over the entire observation period (18 weeks), Akita mice, as expected, developed hyperglycemia (blood glucose  $\geq 300$  mg/dl) between 4 and 6 weeks of age on standard diet. Compound HBM/Akita mice became hyperglycemic by 7 weeks of age in average, and the degree of hyperglycemia was slightly milder than Akita mice, with significantly lower random blood glucose at multiple time points within the first 12 weeks of age (Figure 4A). Accordingly, the proportion of HBM/Akita mice with random blood glucose  $\geq 300$  mg/dl at 6 weeks was 30%, compared with 90% of Akita mice, whereas all HBM/Akita mice were hyperglycemic by 12 weeks (Figure 4B). Such difference was even clearer when blood glucose was measured after an overnight fast; although all Akita mice were frankly hyperglycemic relative to the other groups at 6 weeks of age, the HBM/Akita double mutants showed normal or slightly elevated overnight fasting blood glucose compared to the nondiabetic groups at this age (Figure 4C). Thus, the HBM mutation delays the onset of hyperglycemia in Akita mice.

ipGTT at 6 weeks of age confirmed reduced glucose tolerance in Akita relative to WT and HBM mice. Glucose tolerance was more variable but significantly better in HBM/Akita relative to Akita mice, although the double mutants remained hyperglycemic up to 2 hours after glucose load (Figure 5A). By contrast, at 8 weeks of age glucose tolerance was equally compromised in both HBM/Akita and Akita mice (Figure 5B), consistent with fasting hyperglycemia in both groups at this age (Figure 4A). Comparison of areas under the curve (AUC) for the ipGTT confirmed delayed development of glucose intolerance in the double HBM/Akita mutants, revealing a larger spread of individual data points in both Akita and double mutants relative to the other two groups at 6 weeks (Figure 5C), but tighter clustering toward higher AUC values

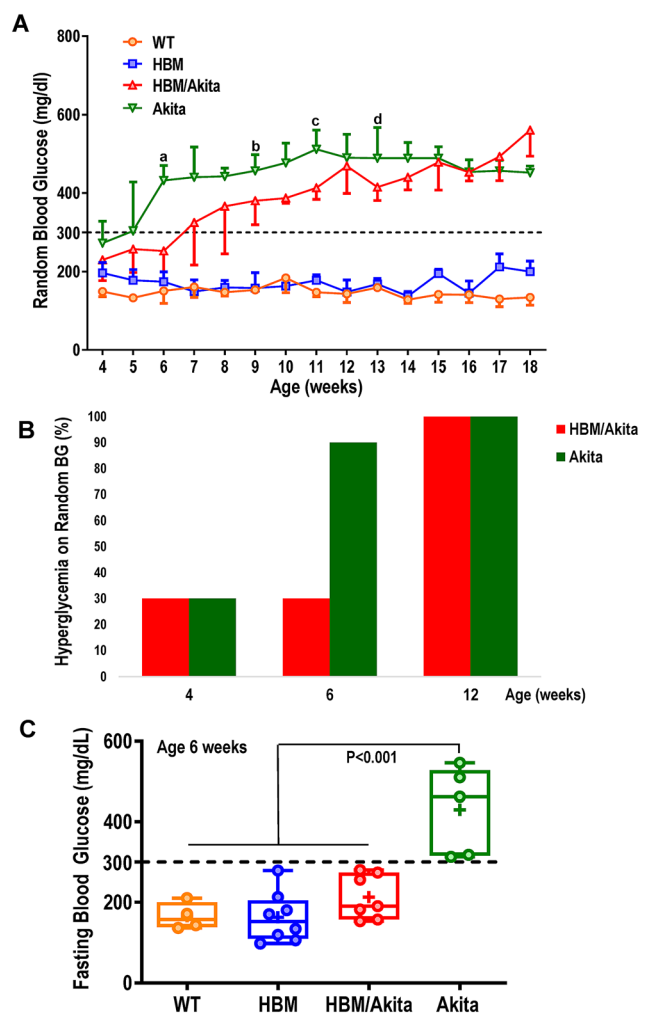


**Fig. 4.** Blood glucose. (A) Random blood glucose (median and interquartile range) measured weekly in the four genotype groups ( $n = 4$ –16 per group at each time point). <sup>a</sup> $p = .025$ , <sup>b</sup> $p = .095$ , <sup>c</sup> $p = .007$ , <sup>d</sup> $p = .052$  versus HBM/Akita (adjusted  $p$  values by Tukey's multiple comparison test after mixed-effect analysis). Akita higher than WT and HBM at all time points ( $p < .01$ ). (B) Percentage of mice with hyperglycemia (random glucose  $> 300$  mg/dl) in HBM and Akita groups at 4, 6, and 12 weeks of age. (C) Fasting blood glucose at 6 weeks of age ( $n = 4$ –8/genotype). Brackets indicate adjusted  $p$  values (Tukey's multiple comparison test) after one-way ANOVA. Abbreviations: ANOVA, analysis of variance; HBM, high bone mass; WT, wild-type.

at 8 weeks (Figure 5D). Notably, at 6 weeks, more than half of HBM/Akita had ipGTT AUC within the normal range, suggesting preserved glucose tolerance in a large proportion of double mutants at this age (Figure 5C). In these experiments, HBM mice, which are heterozygous for the *Lrp5*<sup>A214V</sup> mutation, exhibited normal glucose tolerance (Figure 5A,B). However, homozygous *Lrp5*<sup>A214V/A214V</sup> mutants showed significantly lower blood glucose relative to WT littermates 15 and 30 min after a glucose load (Figure 5, Supplemental Figure S4). The HBM group showed an intermediate response to glucose, suggesting that stronger *Lrp5*-mediated signaling may favor glucose utilization in otherwise healthy conditions.

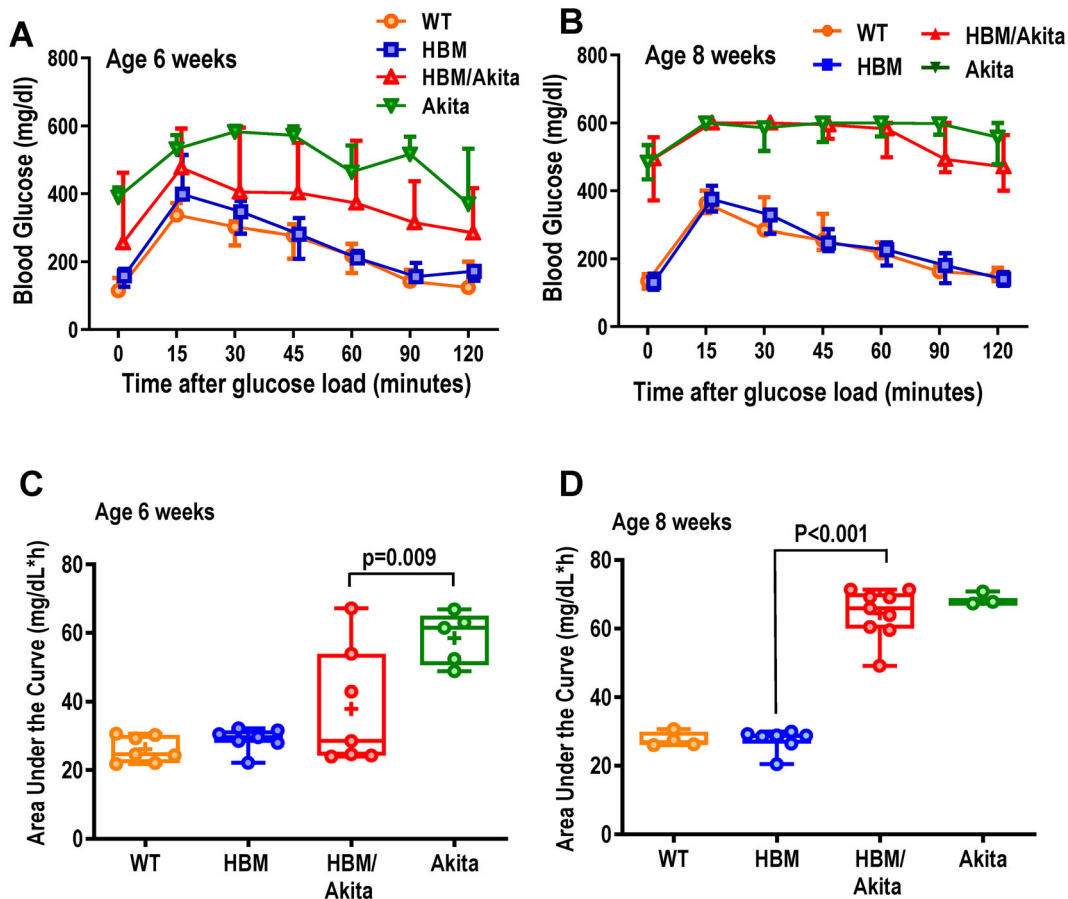


**Fig. 5.** ipGTT. (A,B) Blood glucose before and after an intraperitoneal glucose load (1.5 g/kg) in the four genotype groups at age 6 (WT, HBM, and HBM/Akita,  $n = 7$ ; Akita,  $n = 5$ ) and 8 weeks (WT, Akita,  $n = 4$ ; HBM,  $n = 7$ ; HBM/Akita,  $n = 9$ ). (At 6 weeks:  $p > .10$  at all time points for HBM/Akita relative to all the other groups;  $p < .01$  for Akita relative to WT and HBM [except 120 min, when  $p = .018$ , and  $p = .027$ , respectively]; at 8 weeks:  $p < .001$  for Akita and HBM/Akita vs. WT and HBM at all time points [two-way ANOVA and Tukey's multiple comparison test]). (C,D) Area under the curve for blood glucose during the ipGTT at 6 and 8 weeks of age. Brackets indicate adjusted  $p$  values (Tukey's multiple comparison test) after one-way ANOVA. Pairwise comparisons with  $p > .10$  are not indicated. Abbreviations: ANOVA, analysis of variance; HBM, high bone mass; ipGTT, intraperitoneal glucose tolerance test; WT, wild-type.

### The *Lrp5*<sup>A214V</sup> mutant ameliorates insulin responsiveness in Akita mice without altering insulin production or signaling and independently of osteocalcin

We then performed intraperitoneal ITT (ipITT) in the four groups at 7 weeks, when most of the double mutant mice are not yet hyperglycemic, and at 30 weeks, after a prolonged diabetic status. At 7 weeks, HBM/Akita mice, though already borderline hyperglycemic, exhibited a strong response to insulin with a fast decrease in blood glucose, which remained within or just above the normal range for at least 2 hours after insulin administration. Although hyperglycemic throughout the test, Akita mice also responded to insulin with a significant decline in blood glucose at 60 min, suggesting that they are not insulin insensitive at this age (Figure 6A). At 30 weeks of age, Akita mice showed essentially no response to insulin, consistent with the notion that prolonged hyperglycemia eventually impairs insulin sensitivity. By contrast, insulin was able to decrease blood glucose by more than 30% in the HBM/Akita, even though these mice remained frankly hyperglycemic (Figure 6B). AUC analysis confirmed that

at 7 weeks the Akita group was significantly less responsive to insulin relative to all the other groups, including the HBM/Akita group where a wider spread of data points was observed (Figure 6C). At 30 weeks both Akita and double mutants were significantly less insulin sensitive relative to the non-Akita groups (Figure 6D).

To obtain insights on the potential mechanisms by which onset of hyperglycemia is delayed in HBM/Akita mutants, we first measured glucose regulating hormones at 6 weeks of age, when hyperglycemia has developed in Akita, but not in the double HBM/Akita mutants (Figure 4B). Median fasting serum insulin was lower in HBM relative to WT mice, but statistical analysis showed no differences. As expected, serum insulin increased in both groups 30 min after a glucose load. Conversely, both Akita and HBM/Akita mice showed undetectable serum insulin at time 0 or 30 min after glucose load (Figure 7A). Serum C-peptide followed a similar pattern, with overlapping baseline values in HBM and WT groups, trends to increase after glucose load, and very low levels in both Akita groups at time 0 and 30 min after glucose load (Figure 7B). Circulating glucagon was very low in

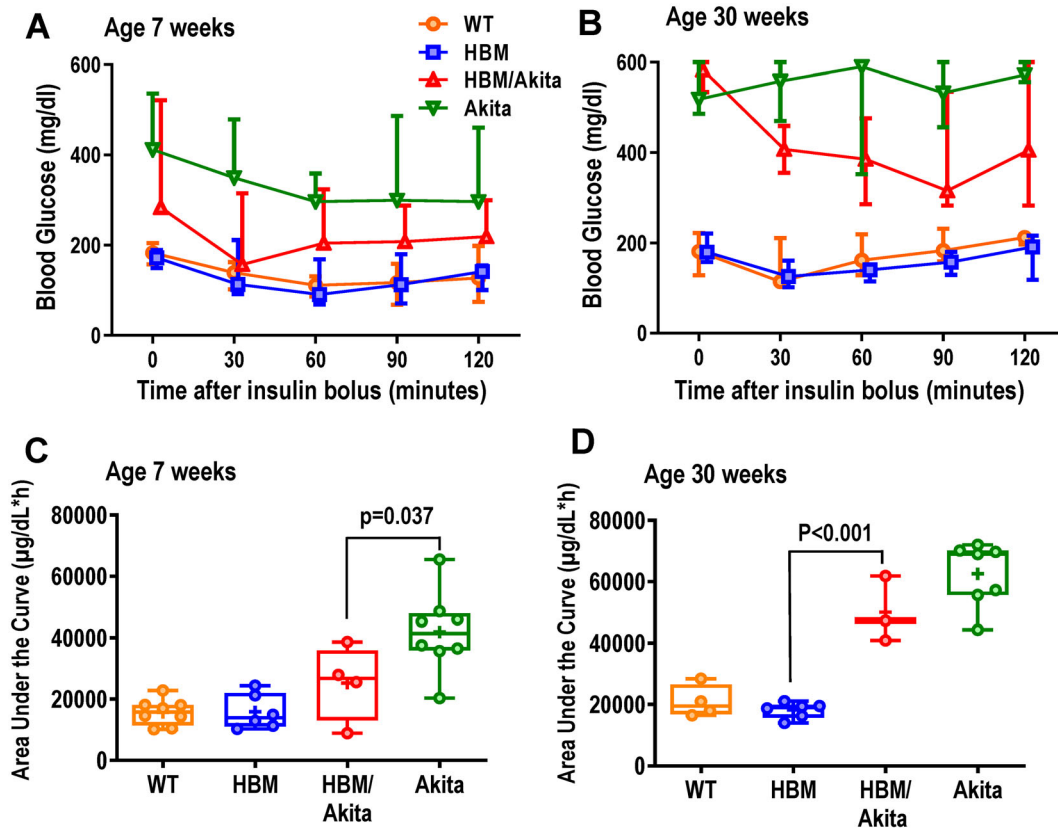


**Fig. 6.** ipITT. (A,B) Blood glucose before and after intraperitoneal injection of insulin (0.5 U/kg) in the four genotype groups at age 7 weeks (WT,  $n = 8$ ; HBM,  $n = 6$ ; Akita, HBM/Akita,  $n = 4$ ) and 30 weeks (WT,  $n = 3$ ; HBM,  $n = 6$ ; Akita,  $n = 7$ ; HBM/Akita,  $n = 3$ ). (At 6 weeks:  $p > .10$  at all time points for HBM/Akita relative to all the other groups;  $p < .01$  for Akita relative to WT and HBM at time points; at 8 weeks:  $p < .001$  for Akita and HBM/Akita vs. WT and HBM at all time-points [two-way ANOVA and Tukey's multiple comparison test]). (C,D) Area under the curve for blood glucose during the ITT at 7 and 30 weeks of age. Brackets indicate adjusted  $p$  values (Tukey's multiple comparison test) after one-way ANOVA. Pairwise comparisons with  $p > .10$  are not indicated. Abbreviations: ANOVA, analysis of variance; HBM, high bone mass; ipITT, intraperitoneal insulin tolerance test; WT, wild-type.

WT and HBM groups, but it was higher in Akita mice before the glucose load, consistent with their hyperglycemia. Notably, serum glucagon was widely variable among the HBM/Akita and Akita groups, with about half of the animals showing frankly elevated levels and a decrease after glucose load only in HBM/Akita mice (Figure 7C). Two other circulating glucose regulating factors were determined. Serum IGF-1 was highly variable in WT and HBM groups, with a decrease after glucose load in WT; and it was barely detectable in both Akita and HBM/Akita groups (Figure 7D). Baseline total osteocalcin, measured at age 28 to 30 weeks, was lower in both Akita and HBM/Akita mice relative to WT and HBM groups (Figure 7E); and Glu13 (undercarboxylated) osteocalcin, which has been proposed as a regulator of glucose homeostasis,<sup>(41)</sup> followed a similar trend (Figure 7F), although higher variability precluded rejection of the hypothesis zero of no differences among groups ( $F = 2.594$ ;  $p = .083$ ). Gla13 (carboxylated) osteocalcin was not different among groups (Supplemental Figure S4B). Of note, similar levels of total and Glu13 osteocalcin were observed in WT and HBM mice.

Because the *Lrp5*<sup>A214V</sup> mutant is globally expressed, we asked whether it may affect insulin production by pancreatic beta cells. Direct measurement of total insulin content in pancreas at 6 weeks of age confirmed barely detectable insulin in any of

the Akita or HBM/Akita double mutant mice at this age, further validating the Akita model; notably, pancreatic insulin content was significantly lower in HBM compared to WT mice (Figure 8A). Finally, we tested insulin responsiveness in extraskeletal and bone cells using pAkt as a readout. In adipocyte cultures obtained from ear mesenchymal stem cells (EMSCs) grown in adipogenic medium, insulin rapidly stimulated Akt phosphorylation to the same extent in both WT and HBM cells, as evidenced by the appearance of strong pAkt bands at 5 and 30 min after insulin exposure in immunoblots, without changes in total Akt abundance (Figure 8B). Identical results were obtained in three replicate experiments using cells from different animals (Figure 8C, Supplemental Figure S5A,B). Consistently, bone marrow stromal cells (BMSCs) from either WT or HBM mice showed similar pAkt activation upon insulin exposure, though to a less extent than EMSC-derived adipocytes (Supplemental Figure 5C).

## Discussion

Our study demonstrates that the *Lrp5*<sup>A214V</sup> mutation results in high bone mass and improves bone microarchitecture and bone strength despite prolonged insulin-deficient diabetes in mice.

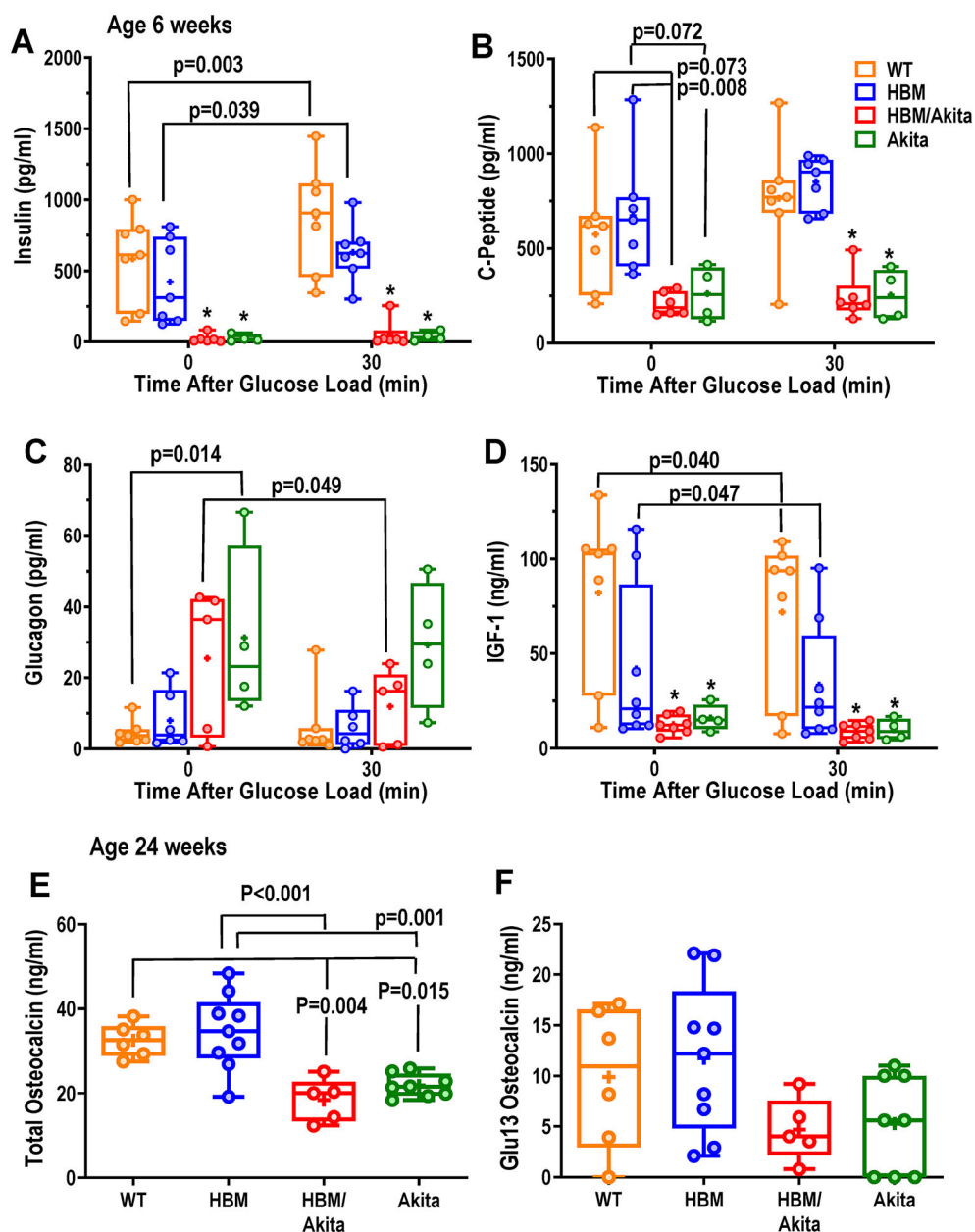


**Fig. 7.** Glucose regulating hormones and osteocalcin. (A) Serum insulin, (B) C-peptide, (C) glucagon and (D) IGF-1 measured before (time 0) and 30 min after a glucose load (i.p. dextrose, 1.5 mg/g) in 6-week-old mice. (E) Serum total and (F) decarboxylated (Glu13) osteocalcin in the four genotype groups at age 28–30 weeks. Brackets indicate adjusted *p* values (Tukey's multiple comparison test) after two-way ANOVA; \**p* < .01 versus WT and HBM at either time point. Pairwise comparisons with *p* > .10 are not indicated. Abbreviations: ANOVA, analysis of variance; HBM, high bone mass; IGF-1, insulin-like growth factor 1; WT, wild-type.

We also show that this mutation delays the onset of diabetes and ameliorates glucose tolerance, primarily via insulin-independent mechanisms. Thus, our work suggests that therapeutic agents based on Wnt signaling activation should be useful in improving bone fragility in patients with diabetes and may have the added benefit of also improving energy metabolism in early stages of the disease.

Despite the severe metabolic imbalance, we found no detectable postnatal developmental or growth defects in Akita mice, at least up to age 20 weeks. This is consistent with previous

observations,<sup>(42,43)</sup> although an age-related reduction in body weight has been reported in older Akita mice.<sup>(44,45)</sup> We did not detect differences in whole-body bone mass or microarchitectural abnormalities in Akita relative to WT mice. Indeed, bone mass in the HBM/Akita compound mutants was as high as in the HBM mutants, and trabecular and cortical bone continued to accrue through at least 20 weeks of age just like in the HBM single mutants. However, others have shown that the effect of hyperglycemia on whole-body bone density is slow and may become evident only at 1 year of age.<sup>(46)</sup> Lack of densitometric

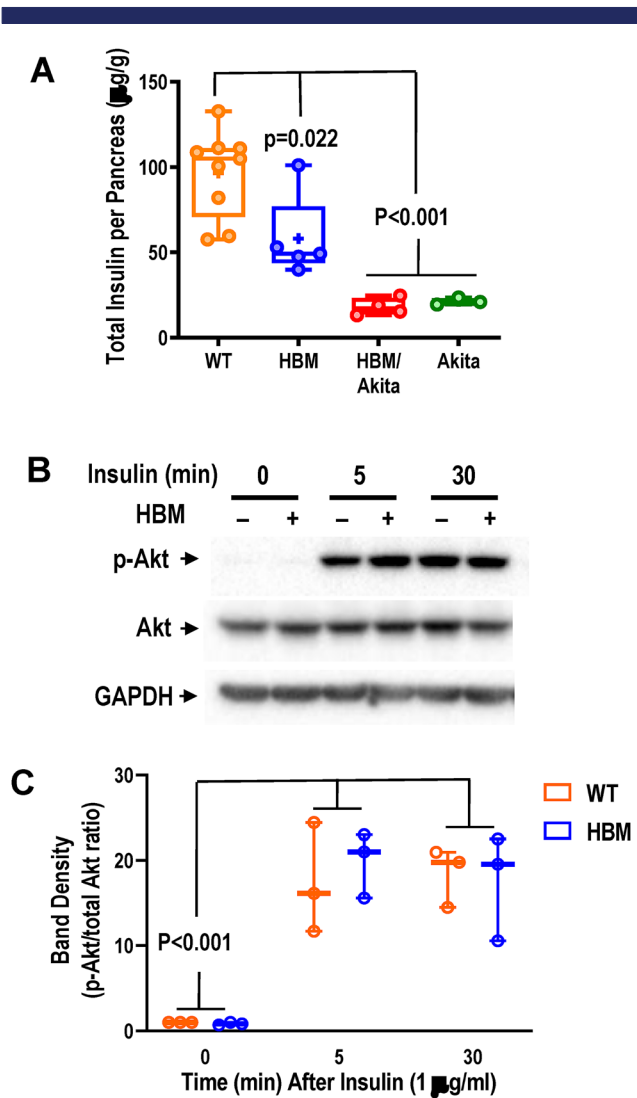


**Fig. 8.** Insulin production and signaling. (A) Total pancreatic insulin content assessed by ELISA in whole pancreas homogenates of 6-week-old mice. Brackets indicate adjusted  $p$  values (Tukey's multiple comparison test) after one-way ANOVA. (B) Immunoblots of whole-cell lysates from ear mesenchymal stem cell-derived adipocyte cultures before and after 5 or 30 min of exposure to 1  $\mu\text{g/ml}$  of insulin. (C) Densitometric analysis of immunoblot bands shown in B and Supplemental Figure S5A,B, expressed as pAKT/total Akt ratio. Brackets indicate adjusted  $p$ -values (Tukey's multiple comparison test) after one-way ANOVA (time,  $F = 33.82$ ,  $p < .001$ ; genotype,  $F = 0.057$ ,  $p = .815$ ; interaction,  $F = 0.252$ ,  $p = .781$ ). Abbreviations: ANOVA, analysis of variance; ELISA, enzyme-linked immunosorbent assay; pAKT, phosphorylated protein kinase B.

or microstructural abnormalities may be considered a limitation of the Akita model; and lack of insulinitis is also a difference with the human disease. On the other hand, with 100% penetrance in males and longtime survival, Akita mice represent an excellent platform to study the effect of prolonged hyperglycemia and insulin deficiency on bone. Indeed, we did detect decreased stiffness in 30-week-old Akita bones, suggesting that prolonged hyperglycemia alters bone material properties rather than bone mass, microarchitecture, or mineralization, probably by abnormal glycosylation of matrix proteins.<sup>(47,48)</sup> More to the point,

conserved bone stiffness and improved bone strength in HBM/Akita relative to Akita mice suggest that the  $Lrp5^{A214V}$  mutation fully overrides any effects of prolonged hyperglycemia and insulin deficiency on bone mass and strength. Intriguingly, high bone mass accrual with the  $Lrp5^{A214V}$  mutation in the Akita background occurs with lower circulating osteocalcin, a marker of bone formation. Such observation is consistent with accumulated clinical evidence that bone formation is reduced in T1DM<sup>(7)</sup>; it also implies that the  $Lrp5^{A214V}$  mutation is more effective in decreasing bone resorption than in counteracting the effect of hyperglycemia on bone formation, to account for the high bone mass. Consistent with this conclusion, in clinical trials the anti-sclerostin antibody, romosozumab transiently stimulates bone formation and reduces bone resorption, but continuous bone mass accrual with prolonged treatment occurs with reduced bone formation and resorption.<sup>(16)</sup>

Other mouse genetic models demonstrate a positive action of Wnt signaling on glucose metabolism. *Sost* knockout mice have improved glucose tolerance and insulin sensitivity and reduced white adipose depots, leading to the suggestion of an endocrine function of sclerostin, which is assumed to be produced only in bone.<sup>(26)</sup> By contrast, *Lrp5* knockout mice have markedly impaired glucose tolerance and decreased glucose-induced insulin secretion.<sup>(25)</sup> As expected, *Lrp5^{A214V}* and *Sost^{-/-}* mice share many similarities in glucose homeostasis, because both mutations result in enhanced Wnt signaling. Glucose tolerance is improved in both, although this is evident only with homozygous  $Lrp5^{A214V/A214V}$  mice in a nondiabetic background. Insulin sensitivity is improved in *Sost^{-/-}* mice, and the  $Lrp5^{A214V}$  mutation also improves insulin sensitivity in a diabetic context, even though it does not affect insulin signaling in bone cells. Furthermore, the reduced pancreatic insulin content in  $Lrp5^{A214V}$  mutants is consistent with reduced beta cell area and size observed in *Sost^{-/-}* mice.<sup>(26)</sup> The reason for reduced insulin content in Wnt signaling gain-of-function mutants remains elusive. Intriguingly, insulin-dependent glucose uptake is increased in *Sost^{-/-}* mice,<sup>(26)</sup> suggesting lower insulin requirement. There are also differences between the two models; unlike the reduced WAT depots in *Sost^{-/-}* mice, the  $Lrp5^{A214V}$  mutation does not alter body adiposity. Further, Akt activation in response to insulin is not altered in cultured  $Lrp5^{A214V}$  adipocytes and BMSC relative to WT cells, whereas enhanced insulin signaling was reported in *Sost* knockout cells.<sup>(26)</sup> Lack of effect of  $Lrp5^{A214V}$  on WAT mass may be explained by recent findings that sclerostin favors adiposity via binding to Lrp4<sup>(49)</sup>; thus, this endocrine action of sclerostin may not require canonical, Lrp5-mediated Wnt signaling. Of note, the  $Lrp5^{A214V}$  mutation renders the receptor sclerostin-insensitive,<sup>(28)</sup> but not capable of ligand-independent signaling; therefore, our data would support the hypothesis that improved glucose metabolism is related to resistance to the inhibitory action of sclerostin in different peripheral tissues, thus reinforcing the notion that sclerostin acts in an endocrine fashion to regulate glucose metabolism and adiposity.

Although insulin-stimulated glucose utilization is improved in HBM/Akita mice, delayed onset of diabetes cannot be mediated by increased insulin production or sensitivity, because not only is insulin abundance reduced in the pancreas of HBM mice, but HBM/Akita mutants remain able to respond to glucose load for 2 to 3 weeks after their beta cell functionality is completely lost. Thus, an insulin-independent mechanism allows  $Lrp5^{A214V}$  mutants to support glucose homeostasis for the first few weeks after insulin failure, though such mechanism is obviously not sufficient to prevent insulin-deficient diabetes. Undercarboxylated

osteocalcin can function as a glucose regulatory factor,<sup>(50,51)</sup> and circulating osteocalcin has been reported elevated in subjects with gain-of-function *LRP5* mutations.<sup>(12)</sup> Although we have not measured osteocalcin at the onset of the metabolic abnormalities, the lower-than-normal osteocalcin in HBM/Akita mice is the opposite of what would be expected if osteocalcin were the mechanism of improved glucose tolerance in these mice. Likewise, circulating undercarboxylated osteocalcin and adiponectin are normal in *Sost*<sup>-/-</sup> mice.<sup>(27)</sup> The surprisingly larger BAT depots in HBM/Akita mutants, in the face of decreased WAT, and more so, prevention of BAT whitening by the *Lrp5*<sup>A214V</sup> mutation in the Akita background, may hold the key to this unexpected finding. Transplantation of normal BAT into streptozotocin-induced diabetic mice restores euglycemia and normal glucose tolerance, and reduces inflammation, independently of insulin.<sup>(52)</sup> Increased production of IGF-1 was proposed as a mechanism; however, IGF-1 was normal in our *Lrp5*<sup>A214V</sup> mutants, even after glucose load, and it was undetectable in both Akita and double mutants. In *Sost*<sup>-/-</sup> mice, BAT mass is normal, although genes associated with adipocyte browning or beiging, such as *Ucp-1* are upregulated in WAT.<sup>(27)</sup> Therefore, it is possible that Wnt signaling may enhance the release of other adipokines or “batokines” with a positive effect on glucose metabolism.

In summary, this study demonstrates that Wnt signaling may provide a common thread between bone and energy metabolism. Activated Wnt signaling improves bone mass, microarchitecture and strength in insulin-deficient diabetes and has positive effects on glucose homeostasis. Diabetes leads to cardiovascular complications, and because there are concerns that romosozumab, an anti-sclerostin antibody, also increases the risk of cardiovascular events, sclerostin inhibition should be considered in subjects with diabetes without complications.

## Acknowledgments

This work was supported by a grant from Società Italiana per l’Osteoporosi e le Malattie del Metabolismo Minerale e Scheletrico (SIOMMMS; to Rocky Strollo), from Fondazione Diabete Ricerca-AMD and Società Italiana di Diabetologia (AMD-SID; to Giulia Leanza), and by a grant from the Barnes-Jewish Foundation (to Roberto Civitelli), and National Institutes of Health (NIH) DK098584 (to Maria S. Remedi). Further support was provided by National Institutes of Health (NIH) P30 AR057235 (Core Center for Musculoskeletal Biology and Medicine). We are grateful to Yung Kim and Michael Brodt for their assistance with the bone biomechanics experiments and analysis.

Author contributions: Giulia Leanza: Conceptualization; data curation; funding acquisition; investigation; methodology; project administration; writing-original draft. Francesca Fontana: Conceptualization; data curation; formal analysis; investigation; methodology; supervision. Seung-Yon Lee: Data curation; formal analysis; investigation; methodology. Maria Remedi: Data curation; formal analysis; investigation; supervision. Celine Schott: Data curation; investigation. Mathieu Ferron: Data curation; methodology; supervision; writing-review & editing. Malcolm Hamilton-Hall: Data curation; formal analysis; visualization. Yael Alippe: Data curation; investigation; methodology. Rocky Strollo: Conceptualization; funding acquisition; supervision. Nicola Napoli: Conceptualization; data curation; funding acquisition; project administration; supervision; writing-review & editing. Roberto Civitelli: Conceptualization; data curation; formal

analysis; funding acquisition; project administration; supervision; writing-original draft; writing-review & editing.

## Disclosures

All authors have nothing to disclose.

## Peer review

The peer review history for this article is available at <https://publons.com/publon/10.1002/jbmr.4303>.

## Data availability statement

The data that support the findings of this study are available from the corresponding authors upon reasonable request.

## References

- Sellmeyer DE, Civitelli R, Hofbauer LC, Khosla S, Lecka-Czernik B, Schwartz AV. Skeletal metabolism, fracture risk, and fracture outcomes in type 1 and type 2 diabetes. *Diabetes*. 2016;65(7):1757-1766.
- Napoli N, Strollo R, Paladini A, Briganti SI, Pozzilli P, Epstein S. The alliance of mesenchymal stem cells, bone, and diabetes. *Int J Endocrinol*. 2014;2014:690783.
- Weber DR, Haynes K, Leonard MB, Willi SM, Denburg MR. Type 1 diabetes is associated with an increased risk of fracture across the life span: a population-based cohort study using The Health Improvement Network (THIN). *Diabetes Care*. 2015;38(10):1913-1920.
- Napoli N, Conte C, Pedone C, et al. Effect of insulin resistance on BMD and fracture risk in older adults. *J Clin Endocrinol Metab*. 2019;104(8):3303-3310.
- Schwartz AV, Vittinghoff E, Bauer DC, et al. Association of BMD and FRAX score with risk of fracture in older adults with type 2 diabetes. *JAMA*. 2011;305(21):2184-2192.
- Armas LA, Akhter MP, Drincic A, Recker RR. Trabecular bone histomorphometry in humans with type 1 diabetes mellitus. *Bone*. 2012;50(1):91-96.
- Starup-Linde J, Vestergaard P. Biochemical bone turnover markers in diabetes mellitus - a systematic review. *Bone*. 2016;82:69-78.
- Farlay D, Armas LA, Gineyts E, Akhter MP, Recker RR, Boivin G. Non-enzymatic glycation and degree of mineralization are higher in bone from fractured patients with type 1 diabetes mellitus. *J Bone Miner Res*. 2016;31(1):190-195.
- Saito M, Fujii K, Mori Y, Marumo K. Role of collagen enzymatic and glycation induced cross-links as a determinant of bone quality in spontaneously diabetic WBN/Kob rats. *Osteoporos Int*. 2006;17(10):1514-1523.
- Tanaka K, Yamaguchi T, Kanazawa I, Sugimoto T. Effects of high glucose and advanced glycation end products on the expressions of sclerostin and RANKL as well as apoptosis in osteocyte-like MLOY4-A2 cells. *Biochem Biophys Res Commun*. 2015;461(2):193-199.
- Leanza G, Maddaloni E, Pitocco D, et al. Risk factors for fragility fractures in type 1 diabetes. *Bone*. 2019;125:194-199.
- Boyden LM, Mao J, Belsky J, et al. High bone density due to a mutation in LDL-receptor-related protein 5. *N Engl J Med*. 2002;346(20):1513-1521.
- Little RD, Carulli JP, Del Mastro RG, et al. A mutation in the LDL receptor-related protein 5 gene results in the autosomal dominant high-bone-mass trait. *Am J Hum Genet*. 2002;70(1):11-19.
- Napoli N, Chandran M, Pierroz DD, et al. Mechanisms of diabetes mellitus-induced bone fragility. *Nat Rev Endocrinol*. 2017;13(4):208-219.
- Nizioletk PJ, Farmer TL, Cui Y, Turner CH, Warman ML, Robling AG. High-bone-mass-producing mutations in the Wnt signaling pathway result in distinct skeletal phenotypes. *Bone*. 2011;49(5):1010-1019.

16. McClung MR, Grauer A, Boonen S, et al. Romosozumab in postmenopausal women with low bone mineral density. *N Engl J Med.* 2014; 370(5):412-420.
17. Hygum K, Starup-Linde J, Harslof T, Vestergaard P, Langdahl BL. Mechanisms in endocrinology: diabetes mellitus, a state of low bone turnover - a systematic review and meta-analysis. *Eur J Endocrinol.* 2017;176(3):R137-R157.
18. Garcia-Martin A, Rozas-Moreno P, Reyes-Garcia R, et al. Circulating levels of sclerostin are increased in patients with type 2 diabetes mellitus. *J Clin Endocrinol Metab.* 2012;97(1):234-241.
19. Gaudio A, Privitera F, Battaglia K, et al. Sclerostin levels associated with inhibition of the Wnt/beta-catenin signaling and reduced bone turnover in type 2 diabetes mellitus. *J Clin Endocrinol Metab.* 2012;97(10):3744-3750.
20. Hie M, Iitsuka N, Otsuka T, Tsukamoto I. Insulin-dependent diabetes mellitus decreases osteoblastogenesis associated with the inhibition of Wnt signaling through increased expression of Sost and Dkk1 and inhibition of Akt activation. *Int J Mol Med.* 2011;28(3):455-462.
21. Portal-Nunez S, Lozano D, de Castro LF, de Gortazar AR, Nogues X, Esbrit P. Alterations of the Wnt/beta-catenin pathway and its target genes for the N- and C-terminal domains of parathyroid hormone-related protein in bone from diabetic mice. *FEBS Lett.* 2010;584(14): 3095-3100.
22. Gennari L, Merlotti D, Valenti R, et al. Circulating sclerostin levels and bone turnover in type 1 and type 2 diabetes. *J Clin Endocrinol Metab.* 2012;97(5):1737-1744.
23. Piccoli A, Cannata F, Strollo R, et al. Sclerostin regulation, microarchitecture, and advanced glycation end-products in the bone of elderly women with type 2 diabetes. *J Bone Miner Res.* 2020;35(12):2415-2422.
24. Kato M, Patel MS, Levasseur R, et al. Cbfa1-independent decrease in osteoblast proliferation, osteopenia, and persistent embryonic eye vascularization in mice deficient in Lrp5, a Wnt coreceptor. *J Cell Biol.* 2002;157(2):303-314.
25. Fujino T, Asaba H, Kang MJ, et al. Low-density lipoprotein receptor-related protein 5 (LRP5) is essential for normal cholesterol metabolism and glucose-induced insulin secretion. *Proc Natl Acad Sci U S A.* 2003;100(1):229-234.
26. Kim SP, Frey JL, Li Z, et al. Sclerostin influences body composition by regulating catabolic and anabolic metabolism in adipocytes. *Proc Natl Acad Sci U S A.* 2017;114(52):E11238-E11247.
27. Li X, Ominsky MS, Niu QT, et al. Targeted deletion of the sclerostin gene in mice results in increased bone formation and bone strength. *J Bone Miner Res.* 2008;23(6):860-869.
28. Cui Y, Niziolek PJ, MacDonald BT, et al. Lrp5 functions in bone to regulate bone mass. *Nat Med.* 2011;17(6):684-691.
29. Niziolek PJ, MacDonald BT, Kedlaya R, et al. High bone mass-causing mutant LRP5 receptors are resistant to endogenous inhibitors in vivo. *J Bone Miner Res.* 2015;30(10):1822-1830.
30. Yoshioka M, Kayo T, Ikeda T, Koizumi A. A novel locus, Mody4, distal to D7Mit189 on chromosome 7 determines early-onset NIDDM in nonobese C57BL/6 (Akita) mutant mice. *Diabetes.* 1997;46(5): 887-894.
31. Wang MW, Wei S, Faccio R, et al. The HIV protease inhibitor ritonavir blocks osteoclastogenesis and function by impairing RANKL-induced signaling. *J Clin Invest.* 2004;114(2):206-213.
32. Szczesny G, Veihelmann A, Massberg S, Nolte D, Messmer K. Long-term anaesthesia using inhalatory isoflurane in different strains of mice-the haemodynamic effects. *Lab Anim.* 2004;38(1):64-69.
33. Grimston SK, Goldberg DB, Watkins M, Brodt MD, Silva MJ, Civitelli R. Connexin43 deficiency reduces the sensitivity of cortical bone to the effects of muscle paralysis. *J Bone Miner Res.* 2011;26(9):2151-2160.
34. Di Benedetto A, Watkins M, Grimston S, et al. N-cadherin and cadherin 11 modulate postnatal bone growth and osteoblast differentiation by distinct mechanisms. *J Cell Sci.* 2010;123(Pt 15):2640-2648.
35. Silva MJ, Ulrich SR. In vitro sodium fluoride exposure decreases torsional and bending strength and increases ductility of mouse femora. *J Biomech.* 2000;33(2):231-234.
36. Wang Z, York NW, Nichols CG, Remedi MS. Pancreatic beta cell dedifferentiation in diabetes and redifferentiation following insulin therapy. *Cell Metab.* 2014;19(5):872-882.
37. Ayala JE, Samuel VT, Morton GJ, et al. Standard operating procedures for describing and performing metabolic tests of glucose homeostasis in mice. *Dis Model Mech.* 2010;3(9-10):525-534.
38. Remedi MS, Friedman JB, Nichols CG. Diabetes induced by gain-of-function mutations in the Kir6.1 subunit of the KATP channel. *J Gen Physiol.* 2017;149(1):75-84.
39. Ferron M, Wei J, Yoshizawa T, Ducey P, Karsenty G. An ELISA-based method to quantify osteocalcin carboxylation in mice. *Biochem Biophys Res Commun.* 2010;397(4):691-696.
40. Rim JS, Mynatt RL, Gawronska-Kozak B. Mesenchymal stem cells from the outer ear: a novel adult stem cell model system for the study of adipogenesis. *FASEB J.* 2005;19(9):1205-1207.
41. Ferron M, Wei J, Yoshizawa T, et al. Insulin signaling in osteoblasts integrates bone remodeling and energy metabolism. *Cell.* 2010;142(2):296-308.
42. Maresch CC, Stute DC, Ludlow H, et al. Hyperglycemia is associated with reduced testicular function and activin dysregulation in the Ins2(Akita+/-) mouse model of type 1 diabetes. *Mol Cell Endocrinol.* 2017;446:91-101.
43. Han Z, Guo J, Conley SM, Naash MI. Retinal angiogenesis in the Ins2 (Akita) mouse model of diabetic retinopathy. *Invest Ophthalmol Vis Sci.* 2013;54(1):574-584.
44. Coe LM, Zhang J, McCabe LR. Both spontaneous Ins2(+/-) and streptozotocin-induced type 1 diabetes cause bone loss in young mice. *J Cell Physiol.* 2013;228(4):689-695.
45. Vastani N, Guenther F, Gentry C, et al. Impaired nociception in the diabetic Ins2(+/-) Akita mouse. *Diabetes.* 2018;67(8):1650-1662.
46. Botolin S, McCabe LR. Bone loss and increased bone adiposity in spontaneous and pharmacologically induced diabetic mice. *Endocrinology.* 2007;148(1):198-205.
47. Rubin MR, Paschalis EP, Poundarik A, et al. Advanced glycation end-products and bone material properties in type 1 diabetic mice. *PLoS One.* 2016;11(5).
48. Picke AK, Campbell G, Napoli N, Hofbauer LC, Rauner M. Update on the impact of type 2 diabetes mellitus on bone metabolism and material properties. *Endocr Connect.* 2019;8(3):R55-R70.
49. Kim SP, Da H, Li Z, et al. Lrp4 expression by adipocytes and osteoblasts differentially impacts sclerostin's endocrine effects on body composition and glucose metabolism. *J Biol Chem.* 2019;294(17): 6899-6911.
50. Wei J, Ferron M, Clarke CJ, et al. Bone-specific insulin resistance disrupts whole-body glucose homeostasis via decreased osteocalcin activation. *J Clin Invest.* 2014;124(4):1-13.
51. Lacombe J, Al Rifai O, Loter L, et al. Measurement of bioactive osteocalcin in humans using a novel immunoassay reveals association with glucose metabolism and beta-cell function. *Am J Physiol Endocrinol Metab.* 2020;318(3):E381-E391.
52. Gunawardana SC, Piston DW. Reversal of type 1 diabetes in mice by brown adipose tissue transplant. *Diabetes.* 2012;61(3): 674-682.